PHONONIC FREQUENCY COMB GENERATION VIA 1:1 MODE COUPLING IN MoS_2 2D NANOELECTROMECHANICAL RESONATORS

Jaesung Lee[1], Steven W. Shaw[2], and Philip X.-L. Feng[1*]*
[1]Department of Electrical & Computer Engineering, Herbert Wertheim College of Engineering, University of Florida, Gainesville, FL 32611, USA
[2]Department of Mechanical & Civil Engineering, Florida Institute of Technology, Melbourne, FL 32901, USA

2022 IEEE 35th International Conference on Micro Electro Mechanical Systems Conference (MEMS) | 978-1-6654-0911-7/22/$31.00 ©2022 IEEE | DOI: 10.1109/MEMS51670.2022.9699651

ABSTRACT

We report on the experimental demonstration of phononic frequency comb (PFC) generation in atomically thin molybdenum disulfide (MoS_2) resonant nanoelectromechanical systems (NEMS) vibrating near ~50 MHz in the very high frequency (VHF) band. PFC patterns are generated by tuning two close-by resonances with a gate voltage (V_g), and driving them at an anticrossing point, where the two modes are coupled through 1:1 internal resonance. The PFC characteristics are tunable by varying RF driving voltage (v_{drv}) and V_g. We find a threshold of PFC generation at v_{drv} = 550mV and V_g = –6.4V, with relatively wide comb teeth spacing around 2.44 to 2.65MHz. At V_g = –7V, the comb teeth spacing is reduced to 0.63MHz, exhibiting strong tunability of PFC.

KEYWORDS

Phononic frequency comb (PFC), internal resonance, mode coupling, frequency tuning, nanoelectromechanical systems (NEMS), two-dimensional (2D) materials.

INTRODUCTION

Phononic frequency combs (PFCs) are attractive and intriguing as new devices for mechanical frequency conversion, sensing, and precision measurement, following the immense success and impact of their pioneering optical counterparts (OFCs, Nobel Prize in Physics, 2005). A few PFCs have been demonstrated lately by coupling two or more mechanical resonance modes and transferring vibration energy back and forth among coupled modes. To achieve strong coupling between the resonance modes, special conditions such as 1:2 and 1:3 internal resonances [1,2], where nonlinear dynamics facilitates coherent energy transfer between coupled modes, have been employed. Internal resonances can be established when the frequency ratio of two modes is made close to an integer number [1,2,3]. Accordingly, for building PFC and achieving mode coupling conditions, it is desirable to employ devices with wide frequency tunability and rich nonlinearity.

The advent of two-dimensional (2D) materials such as graphene and molybdenum disulfide (MoS_2) has enabled the creation of atomically thin NEMS resonators [4,5,6]. Thanks to their ultrathin suspended structures, these devices are operating in the membrane regime [4,5,6], where their resonance frequencies depend on strain, enabling ultrawide range of frequency tuning, up to $\Delta f/f$ ~430% [6]. Frequency tuning in 2D NEMS has been widely achieved via electrostatic forces induced by a gate voltage V_g, and the resonance frequency can be adjusted to lower or higher values through capacitive softening (at low $|V_g|$) or stiffening (at high $|V_g|$, stretching dominates) effects [5,6]. The exceptional frequency tunability of 2D NEMS resonators [5,6] shall facilitate accessing internal resonance conditions and mode coupling, thus they are well suited for building novel, tunable PFCs. In this work, we employ an electrostatically tunable four-layer (4L) MoS_2 NEMS resonator and demonstrate PFC generation using coupled resonance modes via 1:1 internal resonance. We attain the 1:1 internal resonance by tuning the resonance frequencies of two modes that are close-by initially. By introducing a single-frequency driving signal around the anticrossing point of coupled modes, a PFC is generated, and the intriguing characteristics and tunability of PFC patterns are investigated under different driving conditions.

DEVICE FABRICATION

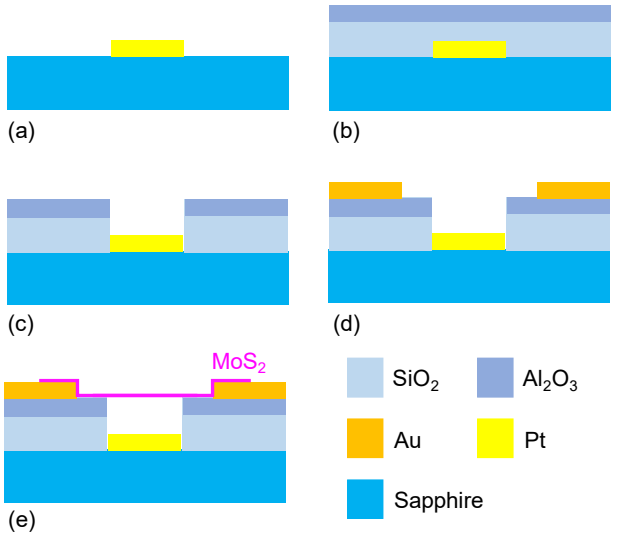

Figure 1: Fabrication process of the MoS_2 2D NEMS resonator. (a) Creation of local gates on a 4-inch sapphire substrate. (b) Deposition of SiO_2 and Al_2O_3 dielectric layers on the sapphire substrate with local gates. (c) Patterning of microtrenches using RIE. (d) Deposition of source and drain electrodes. (e) Dry transfer of MoS_2 flakes onto prepatterned cavities.

We design and fabricate electrostatically tunable circular drumhead 2D NEMS resonators with local gates [7]. A 4-inch insulating sapphire wafer is employed as a substrate to minimize undesirable RF signal crosstalk. First, we pattern local gates (23nm Pt on 2nm Ti) for electrostatic control (Fig. 1a). Next, 300nm SiO_2 and 20nm Al_2O_3 dielectric layers are grown on top of the local gates using plasma enhanced chemical vapor deposition (PECVD) and atomic layer deposition (ALD), respectively, to ensure good electrical insulation between the local gates and NEMS devices (Fig. 1b). Afterwards,

we pattern microcavities using reactive ion etching (RIE) (Fig. 1c). Subsequently, we deposit source and drain electrodes (30nm Au on 5nm Ti) and contact pads (200nm Au on 5nm Ti) (Fig. 1d). Finally, we dry transfer MoS_2 flakes onto the microtrenches with various diameters (Fig. 1e) to make circular drumhead 2D NEMS resonators.

RESULTS AND DISCUSSIONS

After device fabrication, the number of layers of the suspended MoS_2 flake is confirmed by Raman and photoluminescence (PL) measurements. Figure 2 shows measured Raman and PL spectra obtained from the suspended region of the device. The device shows a separation of E^1_{1g} and A_{1g} Raman peaks of 24.3cm^{-1}, indicating clear signatures of four-layer (4L) MoS_2 (Fig. 2a) [8]. The measured PL spectrum exhibits pronounced indirect band transition around ~900nm (Fig. 2b) [9], also verifying the suspended MoS_2 membrane is 4L. We also observe a sharp PL peak at ~694nm, which is attributed to emission from the sapphire substrate.

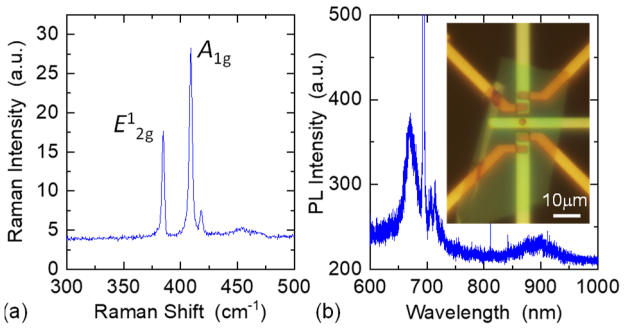

Figure 2: Raman and photoluminescence (PL) signatures of a 4L MoS_2 NEMS resonator. Measured (a) Raman and (b) PL spectra from the suspended region, verifying 4L MoS_2. Inset: optical microscope image of the device with a diameter of 2μm and thickness of 2.8nm.

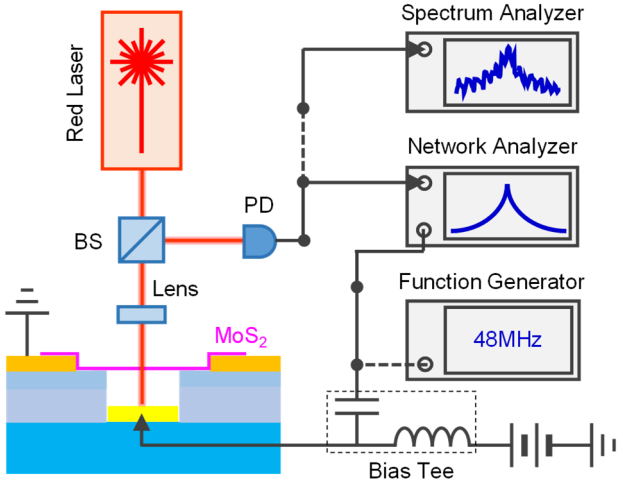

Figure 3: Schematic of laser optical interferometry system. A 633nm red laser light is focused on a suspended MoS_2 membrane. Three measurement configurations are available to detect undriven thermomechanical noise, electrostatically driven resonance, and PFC.

We employ a customized laser interferometry system to characterize the 4L MoS_2 NEMS resonator. A 633nm He-Ne laser is focused onto the suspended MoS_2 circular drumhead using a 50× microscope objective. To avoid any excess laser heating, the laser power is limited to below 300μW on the device. The reflected light modulated by the resonance motion is converted to an electronic signal using a photodetector and measured by using a spectrum analyzer for undriven thermomechanical noise. A network analyzer is used to measure the electrostatically driven resonances. PFC patterns are generated by applying a single-frequency driving signal from a function generator, and measured by using the spectrum analyzer. All the measurements are performed with the MoS_2 device in moderate vacuum ($p \approx$ 10mTorr) and at room temperature ($T \approx$ 300K).

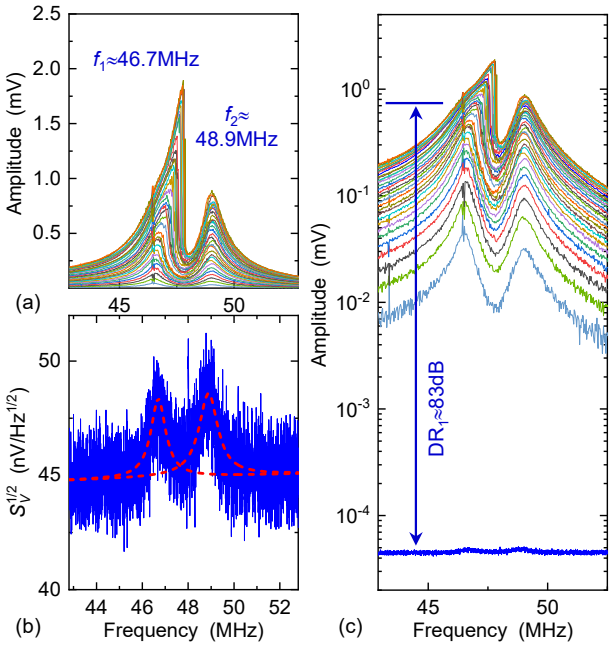

Figure 4: Nonlinearity and DR of the 4L MoS_2 device at V_g = –3V. (a) Driven resonance at varying RF drive v_{drv} = 10–300mV with a 10mV step. (b) Measured thermomechanical noise of the 1st and 2nd modes. Red dashed lines are fitting to a simple harmonic resonator model. (c) Log plot of (a) and (b), showing DR_1 = 83dB.

We first calibrate the two resonance modes of the 2D NEMS resonator, by investigating their basic resonance characteristics, nonlinearity, and dynamic range (DR) [5]. We set V_g = –3V and measure undriven thermomechanical noise without applying v_{drv}. The resonance frequencies and quality (Q) factors of the two modes are determined by fitting the data to a simple harmonic resonator model [4]:

$$S_{x,\mathrm{th}}^{1/2}(\omega) = \left(\frac{4k_B T \omega_n}{M_{\mathrm{eff}} Q} \frac{1}{\left(\omega^2 - \omega_n^2\right)^2 + \omega^2 \omega_n^2 / Q^2} \right)^{1/2} . \quad (1)$$

Here k_B is Boltzmann constant, M_{eff} is the effective mass, ω_n is the angular resonance frequency of n^{th} mode. We find two resonance modes at $f_1 \approx$ 46.7MHz with $Q_1 \approx$ 60, and $f_2 \approx$ 48.9MHz with $Q_2 \approx$ 50 (at V_g = –3V, red dashed lines in Fig. 4b). Next, both V_g and v_{drv} are applied to the gate using a bias tee, and RF drive v_{drv} is gradually increased to study nonlinearity of the resonance modes. For the 1st mode, clear bifurcation is observed under high v_{drv}, showing stiffening Duffing nonlinearity. DR is determined by a ratio of the amplitude at the onset of nonlinearity (*i.e.*, 1dB compression point) to the thermomechanical resonance,

and we obtain $DR_1 \approx 83$dB (Fig. 4c). Meanwhile, the amplitude of the 2nd mode increases linearly with respect to v_{drv}, and it does not exhibit clear Duffing nonlinearity even at $v_{drv} = 300$mV, leading to $DR_2 \geq 85$dB.

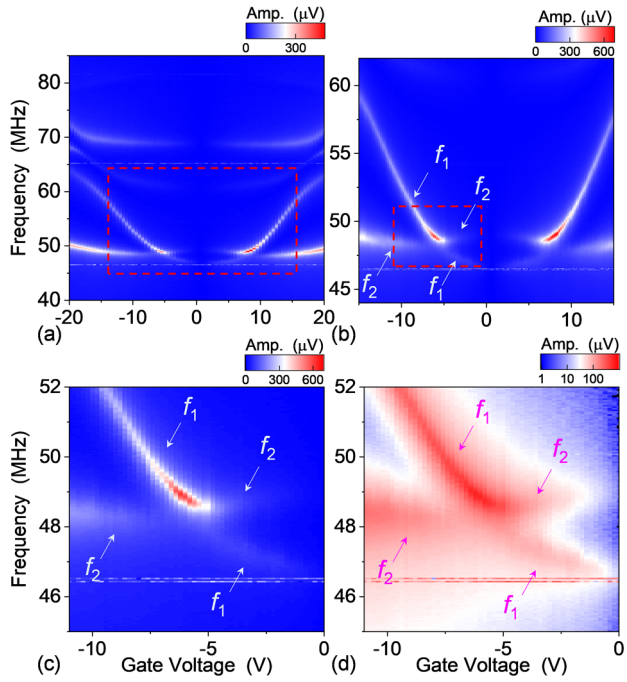

Figure 5: Frequency tuning behavior of the MoS_2 NEMS resonator. 2D color map is constructed by combining measured multimode resonances at varying V_g. The color represents the amplitude of the responses. (a) Frequency tuning map with varying V_g from -20V to 20V with a 0.5V step. (b) Frequency tuning curves in the red box of (a). The resonance curves are measured every 0.2V step. (c) Zoom-in view of red box in (b). (d) Log color scale of data in (c), showing an anticrossing point of the two modes.

To achieve a 1:1 internal resonance condition, we investigate electrostatic frequency tuning of the MoS_2 device by sweeping V_g from −20V to 20V with fixed v_{drv}=10mV. The electrostatic force induced by V_g stretches down the MoS_2 membrane toward the local gate, increasing tension and thus resonance frequency. Meantime, it also introduces capacitive softening effect, which decreases resonance frequency. Interplay between these two effects leads to 'U' or 'W' shaped frequency tuning curves, depending on initial device parameters such as built-in tension and gap between the suspended MoS_2 and the gate [5,6]. In this study, both frequency tuning behaviors are observed from the 4L MoS_2 NEMS resonator (Fig. 5a). As $|V_g|$ changes from 0 to 20V, the 1st resonance mode f_1 exhibits the 'U' shaped tuning curve, and the resonance frequency increases from ~47MHz to ~64MHz, offering frequency tunability of $\Delta f_1/f_1 \approx 36\%$. While the resonance frequency of the 2nd mode is f_2 ~50MHz near $V_g = 0$V, which shifts to ~48MHz at $|V_g|$=10V, and then moves back to ~50MHz at $|V_g|$=20V, showing the 'W' shaped turning curve. The different tuning behaviors in the 1st and 2nd modes bring their resonances to an anticrossing point near $V_g \approx -6$ to −7V (Fig. 5c & 5d), giving lower and upper frequency (energy) branches, and breaking continuity in the f_1 and f_2 tuning curves versus $|V_g|$. As $|V_g|$ increases, the lower (energy) branch assumes mode f_1 and then f_2, while the higher (energy) branch switches from mode f_2 to f_1.

Since energy transfer between coupled modes takes place in the nonlinear regime, we characterize the nonlinear dynamics of the MoS_2 resonator focusing on the 1:1 internal resonance conditions. Based on the frequency tuning maps shown in Fig. 5c and 5d, V_g is set to be −6.4V, and resonance characteristics are measured with varying v_{drv}. At this 1:1 internal resonance setting, we find $f_1 \approx$ 47.3MHz with $Q_1 \approx 100$ and $f_2 \approx$ 48.1MHz with $Q_2 \approx 50$ from the thermomechanical noise (Fig. 6b), showing a frequency splitting of 0.8MHz. Next, we introduce v_{drv} = 5mV to 800mV to the gate with a 15mV step, to excite the resonance motion. Figure 6a shows evolution of the resonance with varying v_{drv}. As v_{drv} increases, the peak point shifts upward in frequency, showing an asymmetric resonance shape (*i.e.*, stiffening Duffing nonlinearity). Even at very high v_{drv} = 800mV, the resonance appears only weakly nonlinear, and the onset of the nonlinearity could be much higher than the measured amplitude. By comparing the measured amplitude at v_{drv} = 800mV with the noise floor, we estimate a measured $DR_1 \geq 102$dB. The surprisingly high DR may be attributed to the interplay of the polarity of Duffing nonlinearity induced by stiffening and capacitive softening effects. Moreover, the results in Fig. 4c and Fig. 6c indicate the MoS_2 device possesses excellent tunability of DR, over 19dB, by controlling V_g.

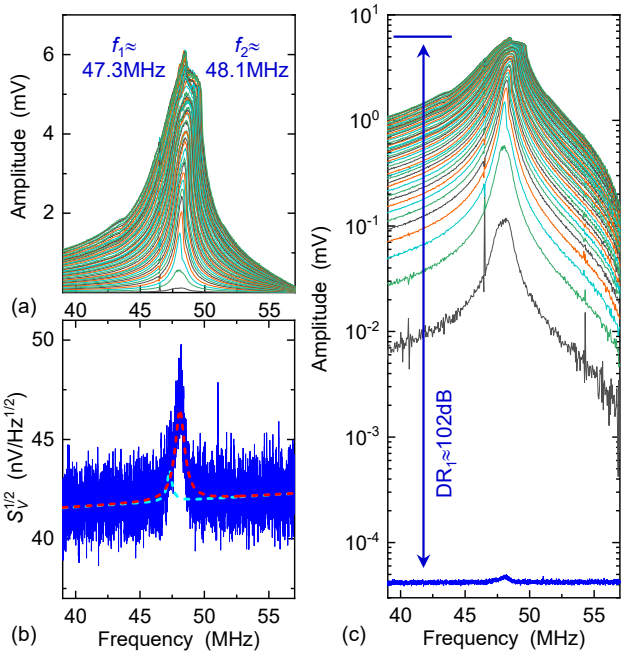

Figure 6: Nonlinearity and DR of the 4L MoS_2 resonator at V_g = −6.4V. (a) Evolution of the driven resonance for v_{drv} = 5mV to 800mV with a 15mV step. (b) Measured undriven thermomechanical Brownian motion of the MoS_2 device. Cyan and red dashed lines are fitting to Eq. 1. (c) The amplitudes from (a) and (b) are plotted in a log scale to clearly show the measured DR of the resonance mode.

We now turn to focus on PFC generation in the MoS_2 NEMS resonator by employing the 1:1 internal resonance mode coupling (Fig. 7a). A single-frequency driving signal near the anticrossing (f_{drv} = 48.06MHz) is applied to the gate with V_g = −6.4V, and PFC spectrum is monitored by

using the spectrum analyzer. No PFC pattern is generated when v_{drv} <550mV (Fig. 7b). Upon v_{drv} >550mV, equally spaced comb teeth appear near f_{drv}, showing a PFC. As the coupled modes start to be weakly nonlinear at v_{drv} = 550mV (Fig. 6a), the PFC generation appears to be related to nonlinearity of the coupled modes. Initially, the measured comb spacing is Δf =2.53MHz at v_{drv} =550mV (Fig. 7b); it increases to Δf =2.65MHz at v_{drv} =570mV (Fig. 7c) and then decreases to Δf =2.44MHz at v_{drv} =650mV (Fig. 7d). The ratio between PFC spacing and drive frequency, $\Delta f/f_{drv}$ =0.055, is much higher than those in PFCs with much larger MEMS resonators ($\Delta f/f_{drv} \approx 10^{-6}$~$10^{-3}$) [1,2]. In the range of v_{drv}>700mV, the PFC pattern gradually disappears as the amplitudes of the comb teeth become smaller.

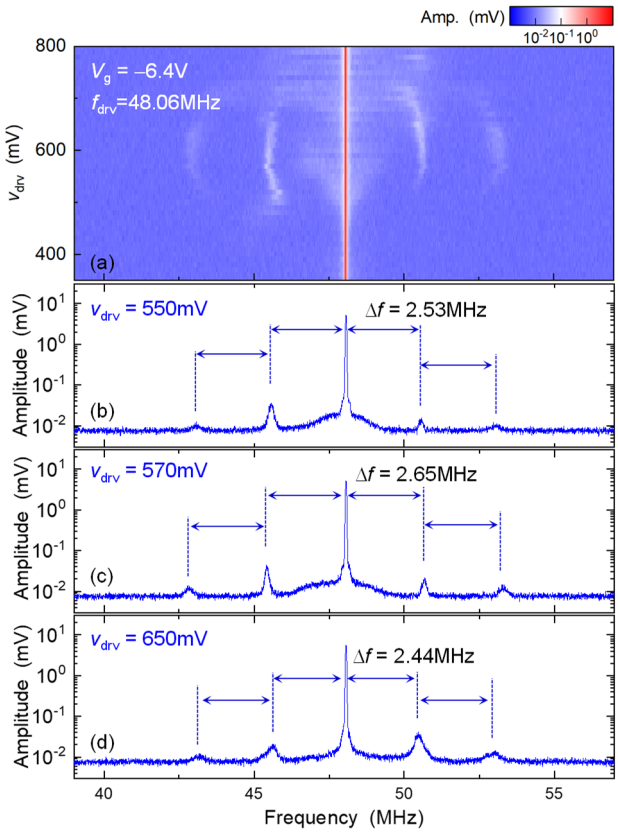

Figure 7: PFC generation in the 4L MoS_2 NEMS resonator. (a) 2D color plot of the PFC at V_g = –6.4V, and f_{drv} = 48.06MHz with v_{drv} = 370mV to 800mV. Examples of the individual PFC spectral responses at (b) v_{drv} = 550mV, (c) v_{drv} = 570mV, and (d) v_{drv} = 650mV.

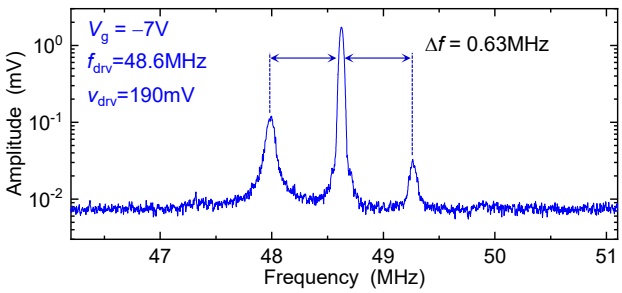

Figure 8: Measured PFC spectral response at V_g= –7V, f_{drv} = 48.6MHz, and v_{drv} = 190mV.

We also investigate the characteristics of the PFC at different V_g. At V_g = –7V with f_{drv} = 48.6MHz and v_{drv} = 190mV, a PFC pattern emerges with Δf = 0.63MHz (Fig. 8). Compared with the PFC patterns demonstrated at V_g = –6.4V, this has narrower frequency spacing. This further shows the strong tunability of the PFC with different V_g and thus the resonance mode coupling conditions.

CONCLUSION

In summary, we have demonstrated PFC generation in an atomically thin MoS_2 NEMS resonator. PFC responses are studied with various excitation and tuning parameters, including V_g, f_{drv}, and v_{drv}. Comparison between the PFC responses and resonance behaviors, including frequency tuning and DR, suggests that the PFC generation is related to 1:1 mode coupling and nonlinearity induced by the input driving signal. The PFC demonstrated and the findings herein will be valuable for applications such as improving sensitivity of resonant sensors and stabilizing oscillators.

ACKNOWLEDGEMENTS

We thank NSF for the support (CAREER Award Grant ECCS-2015708 at UF, Grant CMMI-1662619 at FIT).

REFERENCES

[1] A. Ganesan, C. Do, A. Seshia, "Phononic Frequency Comb via Intrinsic Three-Wave Mixing", *Phys. Rev. Lett.,* vol. 118, Art. No. 033903, 2017.

[2] D. A. Czaplewski, C. Chen, D. Lopez, O. Shoshani, A. M. Eriksson, S. Strachan, S. W. Shaw, "Bifurcation Generated Mechanical Frequency Comb", *Phys. Rev. Lett.*, vol. 121, Art. No. 244302, 2018.

[3] D. Antonio, D. H. Zanette, D. López, "Frequency Stabilization in Nonlinear Micromechanical Oscillators", *Nat. Commun.* vol. 3, Art. No. 806, 2012.

[4] J. Lee, Z. Wang, K. He, J. Shan, P. X.-L. Feng, "High Frequency MoS_2 Nanomechanical Resonators", *ACS Nano,* vol. 7, pp. 6086-6091, 2013.

[5] J. Lee, Z. Wang, K. He, R. Yang, J. Shan, P. X.-L. Feng, "Electrically Tunable Single- and Few-Layer MoS_2 Nanoelectromechanical Systems with Broad Dynamic Range", *Science Advances*, vol. 4, Art. No. eaao6653, 2018.

[6] F. Ye, A. Islam, T. Zhang, P. X.-L. Feng, "Ultrawide Frequency Tuning of Atomic Layer van der Waals Heterostructure Electromechanical Resonators", *Nano. Lett.*, vol. 21, pp. 5508–5515, 2021.

[7] A. Islam, J. Lee, P. X.-L. Feng, "Black Phosphorus NEMS Infrared (IR) Detector", in *Proc. of the 33rd IEEE Int. Conf. on Micro Electro Mechanical Systems (MEMS 2020)*, Vancouver, Canada, January 18-22, 2020, pp. 826-829.

[8] C. Lee, H. Yan, L. E. Brus, T. F. Heinz, J. Hone, S. Ryu, "Anomalous Lattice Vibrations of Single- and Few-Layer MoS_2", *ACS Nano*, vol. 4, pp. 2695–2700, 2010.

[9] K. F. Mak, C. Lee, J. Hone, J. Shan, T. F. Heinz, "Atomically Thin MoS_2: A New Direct-Gap Semiconductor", *Phys. Rev. Lett.*, vol. 105, Art. No. 136805, 2010.

CONTACT

*Jaesung Lee: jaesung.lee@ufl.edu
*Philip Feng: philip.feng@ufl.edu